Quantitative Structure-Activity relationship, Molecular Docking and ADMET Screening of Tetrahydroquinoline Derivatives as Anti-Small Cell Lung Cancer Agents

Ehimen Annastasia Erazua[1], Abel Kolawole Oyebamiji[2+], Sunday Adewale Akintelu[3], Pelumi Daniel Adewole[4], Adedayo Adelakun[5], Babatunde Benjamin Adeleke[1]

1. University of Ibadan, Department of Chemistry, Ibadan, Nigeria.
2. Bowen University, Department of Chemistry and Industrial Chemistry, Iwo, Nigeria.
3. Beijing Institute of Technology, School of Chemistry and Chemical Engineering, Beijing, China.
4. Elizade University, Department of Medical Laboratory Science, Ilara-Mokin, Nigeria.
5. Southeast Iowa Regional Medical Center, Iowa, United States.

+Corresponding author: Abel Kolawole Oyebamiji, Phone: +2348032493676, Email address: abeloyebamiji@gmail.com

Section Editors: Assis Vicente Benedetti

ABSTRACT: Lung carcinoma (LC) is responsible for almost one-third of all cancer fatalities worldwide. Tetrahydroquinoline is an organic molecule that is the semi-hydrogenated derivative of quinoline and could be found in several naturally occurring compounds such as flindersine, oricine etc. Some tetrahydroquinoline derivatives with pyrazole and hydrazide moieties were evaluated in silico against A549 (human lung cancer cell lines). The quantitative structural-activity relationship (QSAR) model created was statistically significant with validation metrics of R^2 (0.9525), R^2adj (0.9314), and CV.R (0.9719). The molecular docking analysis revealed that compound C14 demonstrated the best binding affinity towards the studied protein with binding affinity value of -10.1 kcal mol^{-1} (4LRM). This is in accordance with the experimental result ($IC_{50} = 0.69$). The factors observed for ADME&T correlated well with the factors observed for the referenced drug. This study indicates that compounds C1 and C9 can be further developed as anti-epidermal growth factor receptor (EGFR) compounds. Thus, our findings may open door for the design and development of library of efficient Tetrahydroquinoline-based drug-like compounds as potential anti-LC agents.
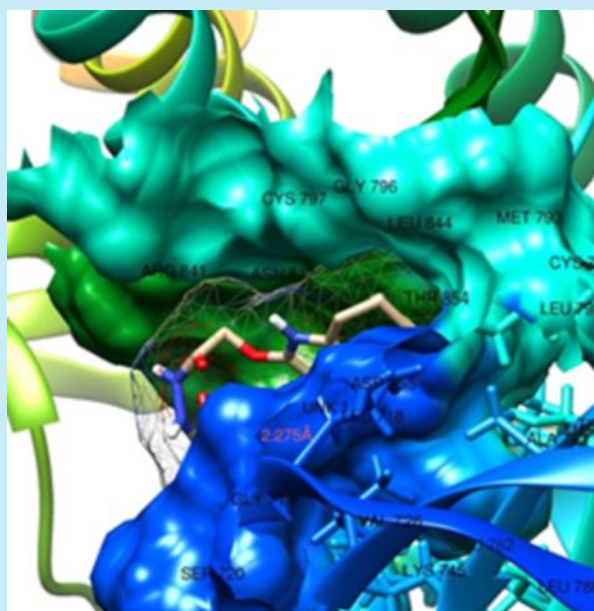
1. Introduction

Lung carcinoma (LC) leads to the greatest number of cancer-associated morbidity and death across the globe (Siegel *et al.*, 2016). It accounted for around one-third of all cancer deaths worldwide (Ibrahim *et al.*, 2020) and is now the fourth most common reason for respiratory disease patients to be admitted to the hospitals (Salim *et al.*, 2011). This disease begins as a primary metastatic tumor in the lungs and escalate to other region of the body. Weight loss, difficulty in breathing, cough (sometimes with blood), and chest pain (Wang *et al.*, 2016) are all known signs of LC. Genetic factors, tobacco use, nutrition, air pollution, and obesity are some of the factors that have been linked to lungs cancer (Cassidy *et al.*, 2008).

Small cell lung cancer (SCLC) and non-small cell lung carcinoma (NSCLC) are the two main types of lung cancer (Collins *et al.*, 2007). NSCLC constitutes 85% of total cases and 40% of NSCLCs are adenocarcinoma (Devesa *et al.*, 2005; Morgensztern *et al.*, 2010). The most effective strategy to treat NSCLC adenocarcinoma is to target the adenosine triphosphate (ATP) binding cleft of the tyrosine kinase binding domain of epidermal growth factor receptor (EGFR) using possible inhibitors (such as gefitinib and erlotinib) (Zhang *et al.*, 2012). However, the establishment of acquired drug resistance in patients restricts its usage in therapeutic settings (Stella *et al.*, 2012). The underlying molecular reason of medication resistance is thought to be steric interferences in the EGFR and inhibitor binding properties caused by mutations. Although irreversible inhibitors such as afatinib and osimertinib were created to combat EGFR molecule acquired resistance, they were discovered to change the covalent connections in the EGFR protein structure, restricting their practical application (Sato *et al.*, 2012). As a result, there is a pressing need to find and develop novel, safe treatment regimens that can quickly overcome medication resistance caused by EGFR mutations.

Quinolines and their derivatives are a class of chemical compounds that have been shown to have a variety of biological actions, including anticancer activity (Hayat *et al.*, 2010; Mekheimer *et al.*, 2020). Tetrahydroquinolines are significant building blocks in the chemical structure of a variety of physiologically active derivatives, such as pyrazolo[3,4-b]quinolines, and have strong anticancer properties (Faidallah and Rostomb, 2013). The quinoline and pyrazole moieties in the pyrazoloquinolines framework are excellent anticancer medicines with a wide range of pharmacological efficacies (Opoku-Temeng *et al.*, 2018). In the creation of anticancer medicines, the quinoline hydrazide scaffold plays a significant role (Mandewale *et al.*, 2017). Currently, there is a lot of interest in pyrazoloquinolines framework physiologically active molecules.

Computational studies based on ligand and structure-based techniques are regarded useful tools in medicinal chemistry for speeding up the drug design process. Molecular docking is a computer-aided drug design process that uses in silico virtual screening to determine how ligands and receptors interact utilizing their specific 3D architectures (Lapa *et al.*, 2013). A drug's drug-likeness, lipophilicity, pharmacokinetic, and toxicity qualities provide information about how the body reacts to its administration. As a result, before this medicine reaches the final (clinical) stage, it must be studied for drug-likeness and pharmacokinetic features.

Therefore, this research was aimed at identifying the descriptors that are responsible for anti-EGFR activities thereby downregulating human lung cancer and developing valid quantitative structural relationship activity (QSAR) model using the obtained descriptors as well as observing the nonbonding interactions between the selected phytochemicals (synthesized by Fathy *et al.*, 2020) and EGFR (PDB ID: 4LRM) (Yasuda *et al.*, 2013).
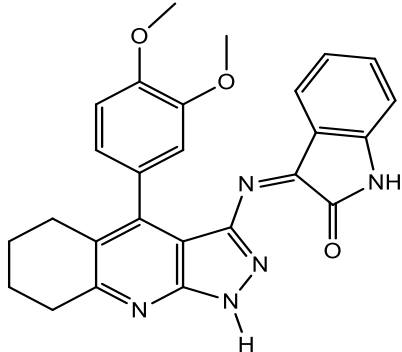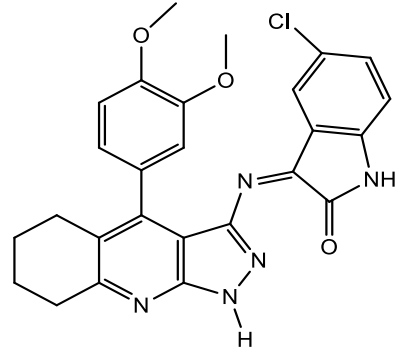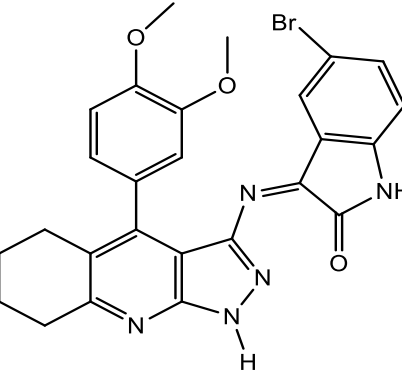
2. Methodology
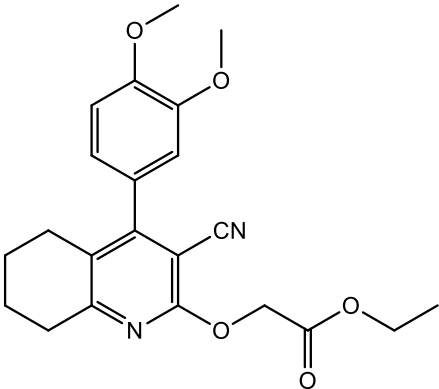
2.1 Quantum Chemical Study
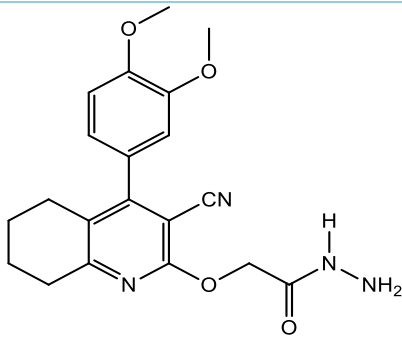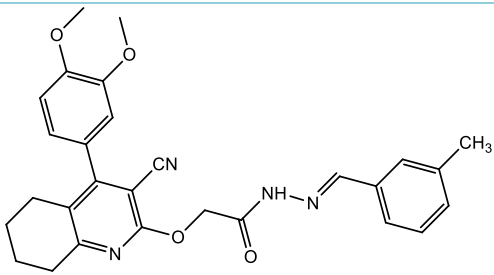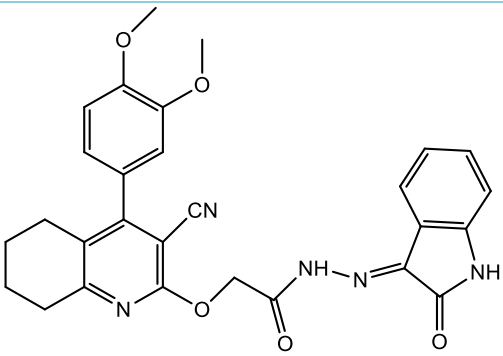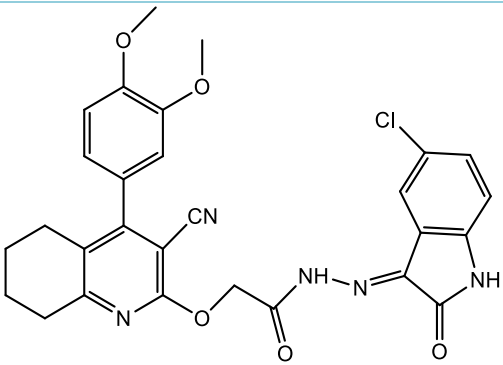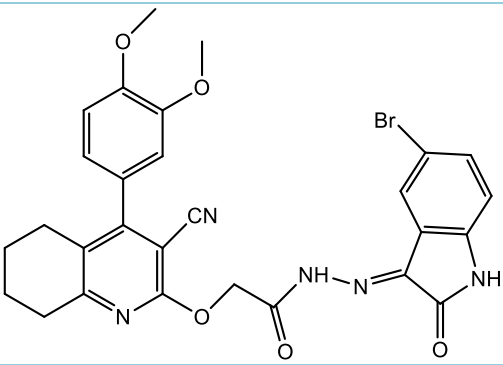
For this study, a set of 14 tetrahydroquinoline derivatives obtained from Fathy *et al.* (2020) as potential anti-EGFR agents with inhibitory activities (IC$_{50}$) in μmol L^{-1} (Table 1) was investigated. All the studied compounds were optimized using Spartan 14 software (Waziri *et al.*, 2023) to achieve a stable conformation with the least amount of energy. Molecular mechanics force field (Vanommeslaeghe *et al.*, 2014) was used to remove the strain energy from the molecules, and density functional theory was used to execute the optimization using the standard 6-31+G* (d, p) basis set, which includes Becke's (1993) gradient, exchange correlation and the Yang *et al.* (2005), Parr *et al.* (1999) correlation functional (i.e., B3LYP).

Table 1. Chemical structure, IUPAC name and IC$_{50}$ of studied compounds.

Code	Chemical structure	IUPAC name	IC$_{50}$ (µmol L^{-1})
C1		2-chloro-4-(3,4-dimethoxyphenyl)5,6,7,8-tetrahydroquinoline-3-car-bonitrile	85.50
C2		4-(3,4-dimethoxyphenyl)-5,6,7,8-tetra-hydro-2H-pyrazolo[3,4-b]quinolin-3-amine	58.60
C3		(E)-4-(3,4-dimethoxyphenyl)-N-(4-(dimethylamino)benzylidene)-5,6,7,8-tetra-hydro-1H-pyrazolo[3,4-b]quinolin-3-amine	17.90
C4		(E)-N-(2,4-dichlorobenzylidene)-4-(3,4-dimethoxyphenyl)-5,6,7,8-tetra hydro-1H-pyrazolo[3,4-b]quinolin-3-amine	35.40
C5		(E)-4-(3,4-dimethoxyphenyl)-N-(3-methylbenzylidene)-5,6,7,8-tetrahydro-1H-pyrazolo[3,4-b]quinolin-3-amine	15.40
			Continue…

C6		(Z)-3-((4-(3,4-dimethoxyphenyl)-5,6,7,8-tetrahydro-1H-pyrazolo[3,4-b]quinoline-3-yl)imino)indolin-2-one	1.37
C7		(Z)-5-chloro-3-((4-(3,4-dimethoxyphen yl)-5,6,7,8-tetrahydro-1H-pyrazolo[3,4-b] quinolin-3-yl)imino)indo lin-2-one	1.20
C8		(Z)-5-bromo-3-((4-(3,4-dimethoxyphenyl)-5,6,7,8-tetrahydro-1H-pyrazolo [3,4-b]quinolin-3-yl)imino)indolin-2-one	1.10
C9		Ethyl-2-((3-cyano-4-(3,4-dimethoxy phenyl)-5,6,7,8-tetrahydroquinolin-2-yl)oxy)acetate	39.60
			Continue…

C10		2-((3-cyano-4-(3,4-dimethoxyphenyl)-5,6,7,8-tetrahydroquinolin-2-yl)oxy)acetohydrazide	4.24
C11		(E)-2-((3-cyano-4-(3,4-dimethoxyphenyl)-5,6,7,8-tetrahydroquinolin-2-yl)oxy)-N'-(3-methylbenzylidene)acetohydrazide	3.10
C12		(E)-2-((3-cyano-4-(3,4-dimethoxyphenyl)-5,6,7,8-tetrahydroquinolin-2-yl)oxy)-N'-(2-oxoindolin-3-yliden e)acetohydrazide	2.00
C13		(E)-N'-(5-chloro-2-oxoindolin-3-ylidene)-2-((3-cyano-4-(3,4-dimethoxyphenyl)-5,6,7,8-tetrahydroquinolin-2-yl)oxy)acetohydrazide	1.06
C14		(E)-N'-(5-bromo-2-oxoindolin-3-ylidene)-2-((3-cyano-4-(3,4-dimethoxylphenyl)-5,6,7,8-tetrahydroquinolin-2-yl)ox y)acetohydrazide	0.69
5-FU		5-flurouracil	0.60

5-FU: 5-Flurouracil.

Source: Fathy *et al.* (2020)

2.3 QSAR Modelling

The obtained descriptors were extracted from the optimized compounds together and were used in developing valid and reliable QSAR model. The extracted descriptors were used as independent variable and the experimental inhibition concentration (IC_{50}) was used as dependent variable. The QSAR model development was achieved using genetic function approximation (GFA) via material studio software (Puzyn *et al.*, 2010) and the MLR-GFA equation for the model is shown in Eq. 1 below:

$$Predicted\ IC_{50} = \alpha + \beta_1 X_1 + \beta_2 X_2 + ... + \beta_n X_n \qquad (1)$$

where α is the regression constant, X_1, X_2.... X_n are the descriptors and β_1, β_2...β_n are the coefficient of the corresponding descriptors. The developed QSAR model was validated by considering series of statistic factors such cross validation R^2 ($CV.R^2$) and Adjusted R^2 (R_a^2) (Eqs. 2 and 3) and the developed model will be considered valid when the calculated value for R_a^2 and $CV.R^2$ were ≥ 0.6 and ≥ 0.5 respectively.

$$CV.R^2 = 1 - \frac{\sum(Yobs - Ycal)^2}{\sum(Yobs - \bar{Y}obs^2)} \qquad (2)$$

where $Yobs$ = experimentally observed IC_{50}, $Ycal$ = calculated IC_{50} and $\bar{Y}obs$ = average of the experimentally observed IC_{50}

$$R_a^2 = \frac{(N-1) \times R^2 - P}{N-1-P} \qquad (3)$$

where N = no of compounds observed, P = no of molecular descriptors used in the QSAR model and R^2 = R- squared value obtained from the QSAR model.

2.4 Molecular Docking

Crystal structure of the EGFR (PDB ID: 4LRM) (Yasuda *et al.*, 2013) was retrieved from the Protein Data Bank (https://www.rcsb.org/) (Yasuda *et al.*, 2013) and employed as target receptors in this study. Also, the tetrahydroquinoline derivatives (Table 1) synthesized by Fathy *et al.* (2020) were used as ligands. The 2D structures of the ligands were drawn with the help of Chem Professional 15.0 and saved as structure-data files (SDFs).

Chimera 1.14 was employed to prepare the protein by eliminating water molecules, numerous ligands, nonprotein component, and other extraneous substances downloaded together with the proteins (Pettersen *et al.*, 2004). The ligands were saved as SDF files and treated protein was converted to PDBQT format using Autodock tool 4.2. Grid box size x = 18.49 Å, y = 22.59 Å, size z = 17.09 Å and grid center dimensions x = 41.77, y = 361.60 and z = 17.09 were set for 4LRM.

The prepared ligands were docked into the binding site of the receptor which was determined by using CastP online server) and the docking calculation was performed using Autodock Vina from PyRX workspace (Trott and Olson, 2010). The inhibitors were treated as flexible throughout the docking simulations. A force-field-based energy scoring function was used to score the ligand orientations, and the highest-scoring binding structure was chosen. Finally, 3D views of the protein-ligand complex were analyzed by using UCSF Chimera 1.14 and Discovery Studio 2020 was used to create the 2D images of the molecular interactions (Capra *et al.*, 2009; Oyeneyin *et al.*, 2022).

2.5 ADMET Screening

The biological action of medications and their metabolic fate in an organism are intimately related to their absorption, distribution, metabolism, and excretion (ADME) and toxicity (ADMET) qualities. In silico predictive models were used to determine the ADMET properties of the test substances. The ADME properties of the substances were determined using the SwissADME online server (http://www.swissadme.ch/index.php/) (Daina *et al.*, 2017). The acute toxicity class, LD50, hepatotoxicity, carcinogenicity, mutagenicity, cytotoxicity, and immunotoxicity of the substances were all predicted using the ProTox-II web server (Banerjee *et al.*, 2018).

The Swiss ADME and ProTox-II online servers take one or more query molecules in canonical SMILES format as input and use a large database to accurately predict the physicochemical properties, pharmacokinetics, solubility, lipophilicity, drug-likeness, bioavailability score, therapeutic properties, and toxicity of compounds.

3. Results and Discussion

3.1 Calculated Descriptors

The calculated descriptors from optimized compounds were screened and for further processing. The calculated descriptors were the energy of the highest occupied molecular orbital (E_{HOMO}), lowest unoccupied

molecular orbital energy (E_{LUMO}), dipole moment (DM), volume, area, lipophilicity (log P), polar surface area (PSA), number of hydrogen bond donor (HBD), hydrogen bond acceptor (HBA). The calculated descriptors also helped in QSAR study. As shown in Table 2, **C3** possess higher E_{HOMO} value and according to report by Semire *et al.* (2017), compound with high E_{HOMO} value possess greater tendency to donate electron

to the neighboring compounds and it is expected to interact with the target; therefore, **C3** with –4.29 eV is expected to interact well with neighboring compounds. As reported by Oyebamiji *et al.* (2018), the lower the E_{LUMO} value the better the tendency of the compound to interact with the target; therefore, **C8** proved to have a tendency to interact than other studied compounds (Table 2).

Table 2. Selected descriptors for the QSAR model.

	E_{HOMO} eV	E_{LUMO} eV	DM debye	MW	Area	Vol	PSA	Log p	Pol	HBD	HBA
C1	–5.27	–2.24	7.73	328.8	339.08	322.96	36.526	1.24	66.86	0	4
C2	–5.03	–1.31	11.48	324.38	340.27	325.26	67.428	–0.16	66.88	2	6
C3	–4.29	–1.99	6.56	455.56	492.87	474.59	54.06	0.66	79.33	1	7
C4	–6.05	–1.99	3.39	481.38	471.57	452.07	52.682	1.12	77.09	1	6
C5	–5.93	–1.78	3.43	426.5	461.31	43.34	52.55	1.66	76.36	1	6
C6	–5.94	–2.54	8.35	453.5	453.91	445.24	79.11	0.56	76.69	2	8
C7	–5.86	–2.91	9.09	487.94	467.07	459.43	79.3	0.42	77.95	2	8
C8	–6.12	–3.78	5.63	532.4	475.79	465.79	80.499	0.69	78.61	2	8
C9	–6.35	–1.67	8.61	396.44	430.16	404.16	62.633	0.64	73.05	0	6
C10	–6.35	–1.66	9.72	382.42	407.97	380.79	98.07	–0.86	71.15	2	8
C11	–6.09	–1.68	8.6	484.56	524.08	498.26	77.218	2.3	80.75	1	8
C12	–5.93	–2.25	13.74	511.54	523.44	501.31	98.47	–0.37	81.17	2	10
C13	–5.92	–2.38	11.48	545.98	533.57	514.42	95.51	–0.51	82.27	2	10
C14	–5.91	–2.39	11.62	590.43	536.62	518.51	94.66	–0.24	82.6	2	10

DM: dipole moment; MW: molecular weight; Vol: volume; PSA: polar surface area; POL: polarizability; HBD: hydrogen bond donor and HBA: hydrogen bond acceptor.

3.2 QSAR Study

Five distinct models were developed and the best model was chosen and reported among them, since it met the minimum conditions for the evaluation of a valid

QSAR model, as reported by Veerasamy *et al.* (2011). Tables 2–5 as well as Figs. 1 and 2 present the findings of the QSAR study and the developed QSAR model was presented in Eq. 4. The selected and reported model is given by the Eq. 4 with the following validation terms: $R^2 = 0.9525$, adj.$R^2 = 0.9314$ and CV.$R^2 = 0.9719$.

$$\text{Predicted IC}_{50} = 179.0741 + 6.54433 \, (DM) - 5.73413 \, (Log\ P) - 28.2133 \, (HBA) + 0.215819 \, (MW) \tag{4}$$
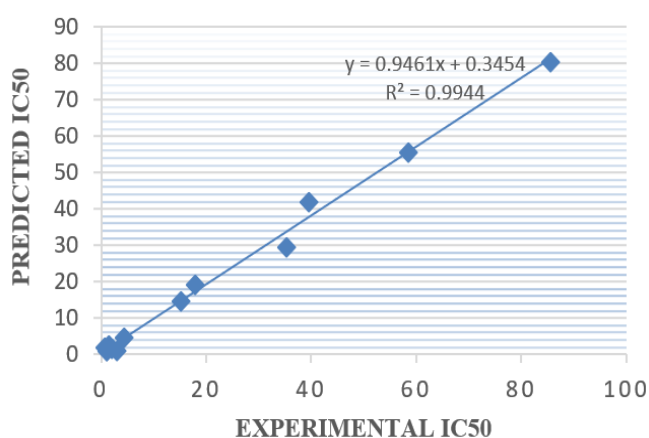

Figure 1. Scatter plot of predicted IC$_{50}$ versus the experimental IC$_{50}$ for the reported model.
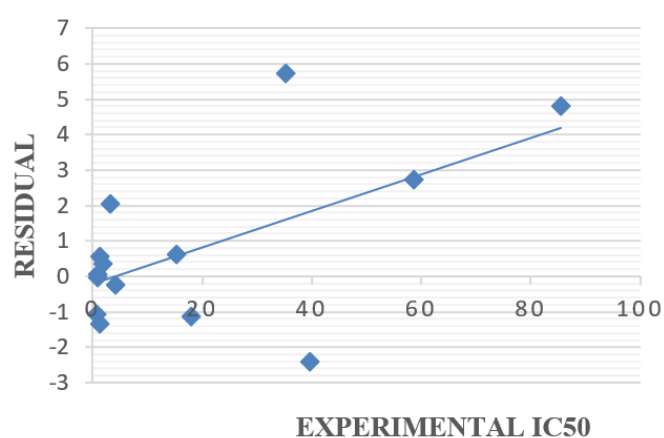

Figure 2. Scatter plot of residual versus the experimental IC$_{50}$ for the reported model.

The negative coefficients of the Log P and HBA descriptors clearly suggested that they have a negative contribution to the compounds inhibitory actions. This suggests that reduction in the amount of these independent descriptors improves the inhibition concentration of the studied compounds, and vice versa. The positive coefficients of dipole moment and molecular weight in the model, on the other hand, indicated that these independent descriptors contributed positively to the inhibitory effects of the ligands under study. It suggests that by increasing the amount of these descriptors in the structures with potential anti-EGFR therapeutic agents, the inhibition concentration these drug-like compounds increases and vice versa (Ibrahim *et al*., 2020; Oke *et al*., 2022).

Also, as reported by Oyebamiji *et al*. (2021), inhibition concentration of any developed QSAR model is not enough to judge the potency of such model and this therefore called for validation of the developed QSAR model. The calculated factors considered for validation were cross validation ($CV.R^2$) and adjusted squared correlation coefficient ($adj.R^2$).

Table 3. Statistical parameters and limit needed for the QSAR model assessment.

Statistical Parameters	Details	Accepted Value	Selected model
R^2	correlation coefficient	≥ 0.6	0.9525
R^2_{adj}	Squared correlation coefficient	≥ 0.6	0.9314
CV.R	Cross-validation coefficient	≥ 0.5	0.9719
$CV.R - R^2_{adj}$	Difference between CV.R and R^2	≥ 0.3	0.0405

The validation factors revealed in this study matched the validation parameters in Table 3, indicating that the model created is both predictive and resilient.

For the compounds under examination, Table 4 displays the experimental IC_{50}, predicted IC_{50}, and residual values. The minimal residual values observed between the experimental and predicted IC_{50} in the table validated the model's high anticipated power (meaning that the reported model was reliable with high predicted power). Figure 1 also shows a plot of the predicted IC_{50} versus experimental IC_{50} for the compounds, and the distribution of the predicted IC_{50} and experimental IC_{50} of the compounds along the line reaffirmed the model's dependability. The R^2 values of the internal validation (0.9525) and the plot (0.9944) agreed with one another, confirming the reported model's stability and reliability (Grisoni *et al*., 2018). Furthermore, Fig. 2 shows a scatter plot of residuals against the experimental IC_{50} which the remarkable appearance of both sets of residuals on the plot's top and lower sides confirms that the reported model was free of methodological mistake (systematic deviations).

Table 4. The experimental IC_{50}, predicted IC_{50} and the residual values for the studied compounds.

	Experimental IC_{50}	Predicted IC_{50}	Residual
C1	85.5	80.66	4.84
C2	58.6	55.85	2.75
C3	17.9	19.05	−1.15
C4	35.14	29.45	5.69
C5	15.4	14.77	0.63
C6	1.37	2.68	−1.31
C7	1.2	1.75	0.55
C8	1.1	1.16	−0.06
C9	39.6	42.03	−2.43
C10	4.2	4.44	−0.24
C11	3.1	1.04	2.06
C12	2.0	1.62	0.38
C13	1.06	1.01	0.05
C14	0.69	1.79	−1.10

Table 6 shows the correlation statistical analysis of the independent descriptors in the presented model, which revealed that there is no relationship between the descriptors in the model. This demonstrated the good performance of the descriptors utilized in creating the reported model.

The variation inflation factor (VIF) data were also examined to see if the descriptors employed in the model had any multicollinearity issues. In general, a VIF value of 1 or a value between 1 and 5 indicates that there is no intercorrelation between the descriptors. Nevertheless, if the VIF value is larger than 10, the produced model is

unstable, and the model should be rechecked if desired (Beheshti *et al.*, 2016). Table 5 shows that the VIF values for each descriptor were less than 5, indicating that the descriptors were highly orthogonal to each other and that there was no intercorrelation between them. This demonstrates that the descriptors used to construct the provided model do not have a multicollinearity problem.

A one-way analysis of variance was used to determine the association between the descriptors and each compound's biological activity (ANOVA). Table 5 shows the probability value of each descriptor at the 95% confidence level ($p = 0.05$). As a result, the alternative hypothesis stating that there is a direct relationship between the biological activity of each compound and the descriptor swaying the built model is accepted; however, the null hypothesis stating that there is no direct relationship between the biological activity of each compound and the descriptor swaying the created model is rejected.

Table 5. Statistical parameters that affect the model.

Descriptors	Regression coefficient	P–value (confidence interval)	VIF	Standard error
DM	–4.43867	0.2580	3.297	3.47832
MW	–0.31745	0.5345	3.541	0.476184
HBA	–8.97918	0.4406	4.349	10.7244
Log P	–1.51775	0.8604	2.202	8.19602

Table 6. Coefficient of Pearson's correlation for descriptor in QSAR model.

| Intercorrelation	Constant	DM	MW	HBA	Log P
Constant	225.902				
DM	–10.9752	1.29913			
MW	–0.607345	0.0415951	0.00386242		
HBA	20.7074	–2.59999	–0.197066	11.9110	
Log P	–12.6244	0.728923	–0.0698522	4.41221	10.2917

3.2 Molecular Docking Studies

Molecular docking technique was used to recognize the compounds which bind well to the EGFR pocket. All tested compounds had strong binding affinity with the receptor. They perfectly fit into the active site of the receptor by interacting with the amino acid residue in the active site of the receptor. The protein residues involved in the interaction, types of interaction involved, distance and binding affinity obtained for each complex formed by the studied compounds and standard were displayed in Tables 7 and 8. The protein residues involved in the interaction and type of interactions observed for C14-EFGR complex was also displayed in Fig. 3.

The complexes formed by 4LRM receptor showed good interactions (Fig. 3). The tested compounds showed binding affinity ranging from –4.6 to –10.1 kcal mol^{-1}. According to Adepoju *et al.* (2022), the lower the binding affinity value of any compound, the better the inhibiting ability of such compound; thus, Compound C14 with –10.1 kcal mol^{-1} was observed to have highest tendency to inhibit the studied receptor than other studied compounds. Pi-anion interaction was observed in all the complexes except in compounds C5, C7, C8, and C9. A salt bridge was formed between Asp858, and the nitro group of the ligand in complex formed by compound C12. Complexes formed by compound C4, C6, C8, C11, and C14 showed a pi-sulfur interaction between Cys800 and the respective ligands. Pi-sigma bond was observed for all complexes except for complexes formed by C2, C5, C9, C12 and C13. only the complex formed by C14 had unfavorable acceptor-acceptor interaction. Complexes formed by compound C2, C5, C9, C10, C11, C12, and C14 showed a conventional hydrogen bond while others do not. Other interactions observed in the complexes are carbon hydrogen bond, pi-pi stacked, alkyl and pi-alkyl (Table 7).

Table 7. Binding Interactions and Binding Affinity between Ligands and Receptor 4LRM.

	Hydrogen interaction	Hydrophobic Interaction	ΔG (kcal mol⁻¹)
C1	-	Thr793, Ala743, Cys800, Ser720, Gly724, Gly719, Arg844, Asn845, Asp858, Lys745, Glu762, Leu718, Thr857, Met766, Leu847, Val726	−8.4
C2	Glu762, Asp858	Leu847, Thr793, Thr857, Met766, LEU791, Lys745, Phe859, Ser720, Gly719, Gly724, Arg844, Phe723, Asn845, Ala743, Val726, Leu718,	−8.1
C3	-	Ala743, Val726, Leu847, Leu718, Gly799, Cys800, Gly719, Arg844, Ser720, Gly721, Phe723, Gly724, Asp858, Asn854, Lys745, Met766, Thr857, Thr793,	−8.2
C4	-	Thr857, Thr793, Val726, Leu718, Gly799, Leu847, Gly719, Cys800, Ser720, Arg844, Leu802, Gly724, Asp803, Phe723, Asp840, Asp858, Asn845, Lys745	−8.7
C5	Asp858, Lys745	Lys878, Phe723, Val879, Pro880, Asp840, Leu861, Gly860, Glu762, Ala755, Ile759, Leu747, Glu758, Lys754, Ala722,	−8.0
C6	-	Arg844, Asp803, Cys800, Gly719, Asn845, Leu847, Val726, Ala743, Leu718, Thr857, Lys745, Asp840, Phe723, Gly724, Asp858, Ser720, Gly721	−7.8
C7	-	Asp803, Arg844, Leu802, Cys800, Glu762, Thr857, Leu847, Val726, Leu718, Asp858, Lys745, Gly719, Thr725, Gly724, Ser720, Phe723, Gly721	7.6
C8	-	Arg844, Asp803, Leu802, Cys800, Gly762, Lys 745, Thr857, Val726, Leu847, Leu718, Asp856, Gly719, Gly724, Phe723, Asp840, Asn845, Ser720, Gly721	−8.4
C9	Thr793, Lys745	Met766, Thr793, Asp858, Gly724, Asn845, Arg844, Phe723, Asp840, Gly721, Ser720, Gly719, Val726, Cys800, Leu718, Leu847, Aa743, Thr857	−8.4
C10	Gln794, Met796	Leu795, Leu718, Leu847, Cys800, Gly719, Ser720, Gly724, Arg844, Phe723, Asp858, Asn845, Glu762, Lys745, Met766, Thr857, Val726, Al743, Thr793	−6.9
C11		Glu762, Lys745, Val726, Met766, Thr793, Ala743, Thr857, Arg 844, Cys800, Ser720, Gly724, Asp840, Leu861, Phe723, Asn845, Asp858, Gly719, Leu847	−8.4
C12	Lys745	Cys800, Asn845, Asp858, Gly724, Glu758, Leu747, Leu861, Gly860, Lys878, Pro880, Val879, Phe723, Asp840, Arg844, Val726, Thr857, Leu847	−9.5
C13	Arg844	Thr793, Thr857, Lys745, Glu762, Cys800, Gly724, Asp840, Leu861, Asp858, Phe723, Asn845, Gly721, Ser720, Gy719, Gly799, Ala743, Leu718, Leu847, Leu795, Val726	−9.4
C14	Lys745, Arg844	Thr857, Thr793, Asp858, Asn845, Gly724, Gly860, Ile759, Glu758, Lys878, Leu861, Val879, Pro880, Asp840, Phe723, Gly719, Cys800, Val726, Ala743, leu847 Thr857	−10.1
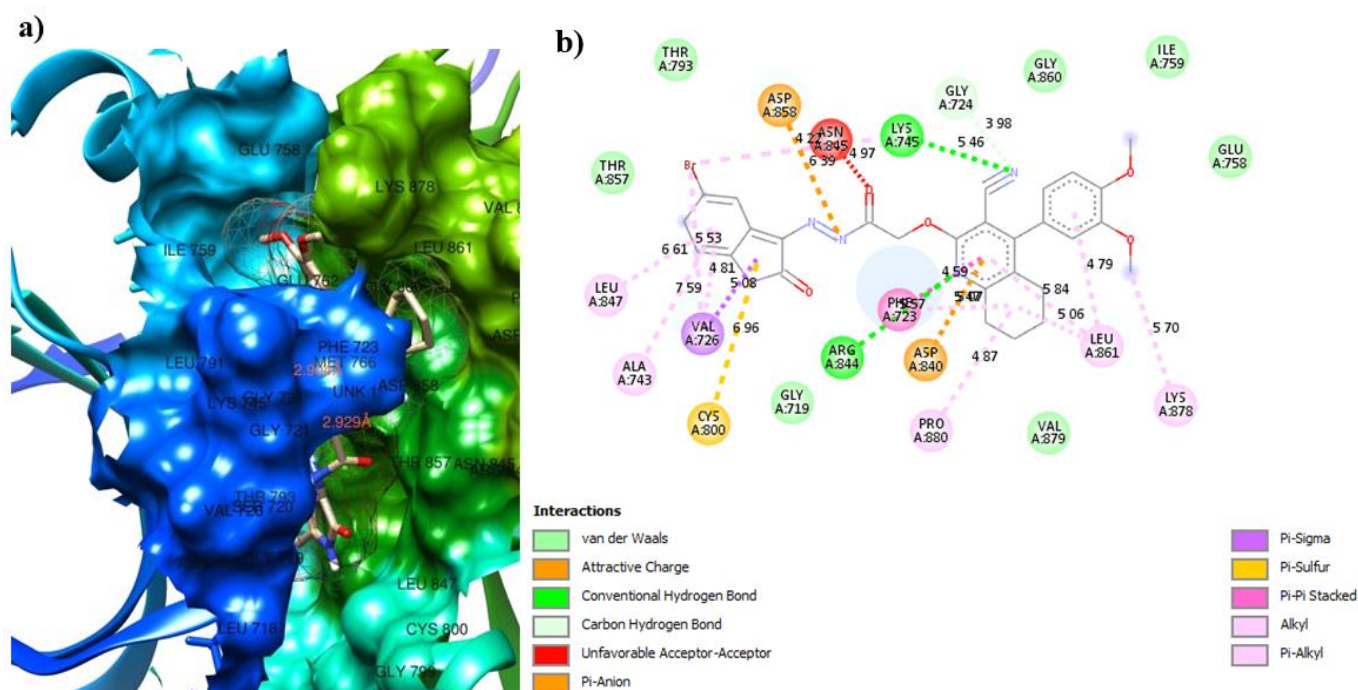
Figure 3. (a) 3D and **(b)** 2D views of the molecular interactions of amino acid residues of receptor 4LRM with compound **14**.

3.3 ADMET Profiling

Regardless of the compounds inhibitory capability against target proteins, the ADMET properties of the compounds are a critical element in determining their pharmacological activities such as drug-likeness, lipophilicity, pharmacokinetics, and toxicity profile when used as drug. In silico ADMET prediction is a quick and low-cost method of determining whether a molecule will be well distributed to its intended site of action, metabolized efficiently, and quickly removed from the body without causing hazardous side effects (Ntie-Kang, 2013). The prediction output for drug likeness, lipophilicity pharmacokinetics, and toxicity profiles of test molecules are displayed on Tables 9–11 respectively.

Drug-likeness analysis is a qualitative evaluation of oral bioavailability based on structural or physicochemical examination of molecules. In this study the rule base filters which include Lipinski's *et al.*

(2013), Veber *et al.* (2002), and Muegge and Ghose (2001) rules were employed to determine if a molecule is impermeable or badly absorbed. If a molecule does not break more than two rules, it is deemed orally bioavailable. As indicated on Table 8, the molecular weights of the compounds range from 130 (5-FU) to 590 g mol^{-1} (C14). The HBA ranged from 3 to 8 and HBDs ranged from 0 to 2; number of rotatable bonds are between 0 (5-FU) to 9 (C11). The TPSA are between 55.14 (5-FU) and 134.93 (C13 and C14). MR ranged from 27.64 (5-FU) to 150.11 (C14). The less the drug candidate can infiltrate, the higher the TPSA and molecular weight values are, and vice versa.

A target molecule's synthetic accessibility (SA) score is used to evaluate it before it is synthesized. It is a parameter used to rate the ease or difficulty of synthesizing a compound. The SA score runs from 1 (very easy) to 10 (very tough) (Swierczewska *et al.*, 2015). The studied compounds possess good SA, with SA scores ranging from 1.52 to 4.13 as shown in Table 8.

Table 8. Drug-likeness prediction output of test compounds.

Sample code	Chemical formula	MW (g mol^{-1})	Rotatable bond	HBA	HBD	TPSA	MR	SA
C1	$C_{18}H_{17}ClN_2O_2$	328.79	3	4	0	55.14	89.81	2.93
C2	$C_{18}H_{20}N_4O_2$	324.38	3	4	2	86.05	94.15	3.11
C3	$C_{27}H_{29}N_5O_2$	455.55	6	5	1	75.63	137.64	4.04
C4	$C_{25}H_{22}Cl_2N_4O_2$	481.37	5	5	1	72.39	133.46	3.82
C5	$C_{26}H_{26}N_4O_2$	426.51	5	5	1	72.39	128.4	3.89
C6	$C_{26}H_{23}N_5O_3$	453.49	4	6	2	101.49	133.76	3.91
C7	$C_{26}H_{22}ClN_5O_3$	487.94	4	6	2	101.49	138.77	3.92
C8	$C_{26}H_{22}BrN_5O_3$	532.39	4	6	2	101.49	141.46	3.97
C9	$C_{22}H_{24}N_2O_5$	396.44	8	7	0	90.67	107.00	3.55
C10	$C_{20}H_{22}N_4O_4$	382.41	7	7	2	119.49	101.81	3.36
C11	$C_{28}H_{28}N_4O_4$	484.55	9	7	1	105.83	137.05	4.02
C12	$C_{28}H_{25}N_5O_5$	511.53	8	8	2	134.93	142.41	4.06
C13	$C_{28}H_{24}ClN_5O_5$	545.97	8	8	2	134.93	147.42	4.06
C14	$C_{28}H_{24}BrN_5O_5$	590.42	8	8	2	134.93	150.11	4.13
5-FLU	$C_4H_3FN_2O_2$	130.08	0	3	2	65.72	27.64	1.52

5-FLU: 5-flurouracil; MW: molecular weight; MR: molar refractivity; HBA: hydrogen bond acceptor; HBD: hydrogen bond donor; TPSA: topology polar surface area; MR: molar refractivity; SA: synthetic accessibility.

The partition coefficient between n-octanol and water (log Po/w) is the fundamental descriptor for lipophilicity (Log P). The tested compounds' log P values, water solubility, and bioavailability are reported in Table 9. Lipophilicity and water solubility are two important physicochemical qualities that influence a drug's behavior. An orally delivered medicine should be lipophilic enough to pass through the intestinal lining, permeate target cell membranes, and be hydrophilic enough to move through the aqueous blood. The higher a compound's log P value, the more lipophilic it is and the less water soluble it is (Johnson *et al.*, 2021). The log P values for the studied compounds ranged from

–0.13 (5-FU) to 5.77 (C4), which revealed that C4 is not as soluble as the referenced drug (Table 9).

The Silicos-IT prediction model was used to calculate water solubility as the logarithm of molar solubility in water (log S). The log S value of a drug affects its capacity to dissolve, and the lower the value, the better (Darvas *et al.*, 2002). The compounds had log S values ranging from –0.76 (poorly soluble, C4) to –3.5 (soluble, C10) indicating. This trend is in accordance with the values of log P earlier discussed.

The bioavailability score employs the total charge, the TPSA, and the Lipinski filter to provide a semiquantitative indication of the compounds'

likelihood of being effective oral medicines (Testa and Krämer, 2009). The less the drug candidate can penetrate, the higher the TPSA and molecular weight values are, and vice versa. The bioavailability score of the test compounds is 0.55, which means that these compounds have a 55% chance of a minimum of 10% oral absorption in rat or human colon carcinoma (Caco-2) permeability (Testa and Krämer, 2009) indicating that they could be useful as oral drug.

Table 9. Predicted lipophilicity (Log P) values, water solubility and bioavailability of the studied compounds.

Sample code	iLOGP	XLOGP3	WLOGP	MLOGP	Silicos-IT Log P	Consensus Log P	ESOL Log S	Solubility Class	BS
C1	3.13	4.33	4.17	2.23	5.03	3.78	–4.79	Moderately soluble	0.55
C2	2.08	3.27	3.11	2.17	3.64	2.85	–4.18	Moderately soluble	0.55
C3	3.45	5.37	5.34	3.96	6	4.82	–6.11	Poorly soluble	0.55
C4	3.15	6.5	6.58	5.03	7.58	5.77	–7.06	Poorly soluble	0.55
C5	3.25	5.61	5.58	4.29	6.83	5.11	–6.17	Poorly soluble	0.55
C6	2.18	4.58	4.02	3.31	5.62	3.94	–5.73	Moderately soluble	0.55
C7	2.46	5.21	4.68	3.78	6.26	4.48	–6.33	Poorly soluble	0.55
C8	2.35	5.27	4.78	3.88	6.3	4.52	–6.64	Poorly soluble	0.55
C9	3.44	3.96	3.46	1.6	4.72	3.44	–4.57	Moderately soluble	0.55
C10	2.46	2.27	1.88	0.78	2.77	2.03	–3.5	Soluble	0.55
C11	3.44	5.02	4.35	2.16	6.04	4.2	–5.78	Moderately soluble	0.55
C12	2.51	4.53	2.8	1.22	4.83	3.18	–5.69	Moderately soluble	0.55
C13	2.91	5.16	3.45	1.68	5.48	3.74	–6.29	Poorly soluble	0.55
C14	2.74	5.23	3.56	1.78	5.52	3.77	–6.61	Poorly soluble	0.55
5-FU	0.44	-0.89	-0.38	-0.32	1.78	0.13	–0.58	Very soluble	0.55

5-FLU: 5-flurouracil; BS: bioavailability score.

Table 10 showed the result of pharmacokinetics prediction of the test molecules. P-glycoprotein (P-gp), a well-studied plasma membrane ATP-binding cassette transporter, is responsible for the active efflux of xenobiotics through biological membranes to protect the body against foreign substances. This efflux pump contributes to drug resistance by preventing some medications from entering sensitive regions. Except for C13 and C14, all the chemicals had a high likelihood of being absorbed in the gastrointestinal tract. This shows that when these chemicals are taken orally, they have the potential to be absorbed in the gastrointestinal tract (Lynch and Price, 2007).

The enzyme cytochrome P450 monooxygenase plays an important role in the metabolism and removal of drugs. It is a group of isoenzymes that catalyzes several processes in the first phase of drug metabolism (Hollenberg, 2002). The suppression of five main isoforms (CYP1A2, CYP2C19, CYP2C9, CYP2D6, and CYP3A4), which are substrates of 50–90% of medications and primary sources of pharmacokinetics-related drug-drug interactions. Because these enzymes are not inhibited, the chemicals have a high chance of being converted and, as a result, of becoming bioavailable when taken orally. Inhibition of the CYP isomers by the substances, on the other hand, can result in poor bioavailability due to failure to be metabolized and severe side effects due to their retention (Sahin and Benet, 2008). Compounds C1, C2, and C9 are potential

inhibitor of CYP1A2 among the tested compounds. All the compounds are potential inhibitor of CYP2C19 except compound C2, C10, and standard 5-FU. As shown in table 10, only compound C2 and 5-FU (referenced drug) were non-inhibitors of CYP2C9 while other studied compounds proved to possess the ability to inhibit CYP2C19. Compounds C1, C2, C3, C6, C9, and C12 are potential inhibitor of CYP2D6 while others are not. All compounds are potential inhibitors of CYP3A4, except compounds C4, C7, C8, 5-FU. It was observed that the standard 5-FU was is not an inhibitor of any cytochrome P450, which suggests that the standard is more likely to be converted and bioavailable after oral delivery than the compounds investigated.

The skin is a selective barrier that allows diverse compounds to permeate through at different rates based on their physicochemical properties (Dixon et al., 2006). Hence, the skin permeability (LogKp) is a key parameter for the evaluation of molecules that might require transdermal administration (Dixon et al., 2006). The more negative the log Kp (with Kp in cm s⁻¹), the less skin permeant is the molecule. As highlighted in Table 10 log Kp (cm s⁻¹) of the test compounds ranged from –7.73 (least permeant) to –4.62 (most permeant).

The skin acts as a selective barrier, allowing various molecules to infiltrate at varied rates depending on their physicochemical qualities (Cheng and Dixon, 2003). As a result, skin permeability (LogKp) is an important characteristic to consider when evaluating compounds

that may need to be administered transdermally. The lower the log Kp (in cm s^{-1}), the less permeant the molecule is to the skin. The test compounds' log Kp (cm s^{-1}) ranged from –7.73 (least permeant) to –4.62 (most permeant), as shown in Table 9. The values indicate that the compounds show low skin permeability.

Table 10. Pharmacokinetics prediction output of test compounds.

Sample code	GI absorption	P–gp	CYP 1A2 inhibitor	CYP2C19 inhibitor	CYP2C9 inhibitor	CYP2D6 inhibitor	CYP3A4 inhibitor	Log Kp (cm s^{-1})
C1	High	No	Yes	Yes	Yes	No	Yes	–5.23
C2	High	Yes	Yes	No	No	Yes	Yes	–5.96
C3	High	Yes	No	Yes	Yes	Yes	Yes	–5.27
C4	High	Yes	No	Yes	Yes	No	No	–4.62
C5	High	Yes	No	Yes	Yes	No	Yes	–4.92
C6	High	Yes	No	Yes	Yes	Yes	Yes	–5.81
C7	High	Yes	No	Yes	Yes	No	No	–5.58
C8	High	Yes	No	Yes	Yes	No	No	–5.81
C9	High	No	Yes	Yes	Yes	Yes	Yes	–5.91
C10	High	Yes	No	No	Yes	No	Yes	–7.02
C11	High	Yes	No	Yes	Yes	Yes	Yes	–5.69
C12	High	Yes	No	Yes	Yes	Yes	Yes	–6.2
C13	Low	Yes	No	Yes	Yes	No	Yes	–5.97
C14	Low	Yes	No	Yes	Yes	No	Yes	–6.19
5–FU	High	No	No	No	No	No	No	–7.73

5-FLU: 5-flurouracil; GI: gastrointestinal; and P-gp: P-glycoprotein.

The toxicity prediction output of the compounds is shown in Table 11. Compounds C8, C12, C13, and C14 fall under the oral toxicity class 5, while other tested compounds fall under oral toxicity class 4. Human hepatotoxicity (H-HT) is a term that describes and illustrates numerous types of liver damage that can lead to the organ failing or death (Cheng and Dixon, 2003). Compounds C10, C11, C12, C13, and C14 were hepatotoxic. Carcinogenicity compounds can damage the genome, the disrupt cellular metabolic processes and cause cancer. Compounds C2, C3, C4, C5, C6, C11, C12 and the standard are carcinogenic. Immunotoxicity is defined as the negative impact of toxic compounds on the functioning of both the local and systemic immune systems. Only compounds C1, C9, C10 and the standard are nonimmunotoxic. The mutagenicity test is used to identify substances that can cause mutations or malignant growth in humans (Loving *et al*., 2009). Compounds C2, C3, C4, C5, C6, and C12 are mutagenic, and only compound C2 is cytotoxic among the test compounds. The study clearly revealed that most of the compounds possess one form of toxicity except for compounds C1 and C9, which did not show any tendency for hepatotoxicity, carcinogenicity, immunotoxicity, mutagenicity and cytotoxicity, indicating that they are safe as possible therapeutic agents. These two compounds did not violate any of the base rule filter, they are moderately soluble and not P-gp substate.

Table 11. Toxicity profiles of test compounds.

Code	C1	C2	C3	C4	C5	C6	C7	C8	C9	C10	C11	C12	C13	C14	5–FU
LD50 (mg kg^{-1})	753	1000	1000	1000	1000	1000	1000	4000	750	750	750	3000	2001	3009	1923
Toxicity Class	4	4	4	4	4	4	4	5	4	4	4	5	5	5	4
Hepatotoxicity	–	–	–	–	–	–	–	–	–	+	+	+	+	+	–
Carcinogenicity	–	+	+	+	+	+	–	–	–	–	+	+	–	–	+
Immunotoxicity	–	+	+	+	+	+	+	+	–	–	+	+	+	+	–
Mutagenicity	–	+	+	+	+	+	–	–	–	–	–	+	–	–	–
Cytotoxicity	–	–	–	–	–	–	–	–	–	–	–	–	–	+	–

5-FLU: 5-flurouracil.

4. Conclusions

Fourteen selected tetrahydroquinoline derivatives having pyrazole and hydrazide moieties were evaluated in silico against human lung cancer cell lines A549. QSAR technique was used to build a model found to be statistically fit with a very high predictive power and the predicted bioactivity represented the experimental results well. Molecular docking analysis showed that compound C14 demonstrated the best binding affinity, but the drug-likeness, pharmacokinetic properties and toxicity profile of the test compounds revealed that compound C1 and C9 are better NSCLC therapeutic agents because they possess better drug-likeness, pharmacokinetic, and toxicity properties. Hence, they are best fit for development into NSCLC therapeutic agents. In addition, experimental validation of in vivo and in vitro assays for ADME traits is required.

Authors' contribution

Conceptualization: Erazua, E. A.
Data curation: Erazua, E. A.; Oyebamiji, A. K.
Formal Analysis: Oyebamiji, A. K.
Funding acquisition: Not applicable.
Investigation: Erazua, E. A.; Oyebamiji, A. K.
Methodology: Akintelu, S. A.; Adewole, D. P.; Adelakun A. O.
Project administration: Adeleke, B. B.
Resources: Erazua, E. A.; Oyebamiji, A. K.
Software: Oyebamiji, A. K.; Adelakun A. O.
Supervision: Adeleke, B. B.
Validation: Oyebamiji, A. K.; Akintelu, S. A.
Visualization: Erazua, E. A.; Adewole, D. P.
Writing – original draft: Erazua, E. A.
Writing – review & editing: Erazua, E. A.; Oyebamiji, A. K.

Data availability statement

All data sets were generated or analyzed in the current study

Funding

Acknowledgments

References

Adepoju, A. J.; Latona, D. F.; Olafare, O. G.; Oyebamiji, A. K.; Abdul-Hammed, M.; Semire, B. Molecular docking and pharmacokinetics studies of *Curcuma longa* (Curcumin) potency against Ebola virus. *Ovidius University Annals of Chemistry* **2022**, *33* (1), 23–35. https://doi.org/10.2478/auoc-2022-0004

Banerjee, P.; Eckert, A. O.; Schrey, A. K.; Preissner, R. ProTox-II: a webserver for the prediction of toxicity of chemicals. *Nucleic Acids Res.* **2018**, *46* (W1), W257–W263. https://doi.org/10.1093/nar/gky318

Becke, A. D. Density-functional thermochemistry. III. The role of exact exchange. *J. Chem. Phys.* **1993**, *98* (7), 5648. https://doi.org/10.1063/1.464913

Beheshti, J.; Bilal, D.; Mackey, T. P.; Limberg, L.; Bartlett, J. C.; Gwizdka, J.; Jocobson, T.; Ishimura, Y. Information literacy: Bridging the gap between theory and practice. Proceedings of the Association for Information Science and Technology, **2016**, *53* (1), 1–6. https://doi.org/10.1002/pra2.2016.14505301019

Capra, J. A.; Laskowski, R. A.; Thornton, J. M.; Singh, M.; Funkhouser, T. A. Predicting protein ligand binding sites by combining evolutionary sequence conservation and 3D structure. *PLoS Comput. Biol.* **2009**, *5* (12), 1000585. https://doi.org/10.1371/journal.pcbi.1000585

Cassidy, A.; Myles, J. P.; van Tongeren, M.; Page, R. D.; Liloglou, T.; Duffy, S. W.; Field, J. K. The LLP risk model: An individual risk prediction model for lung cancer, *Br. J. Cancer* **2008**, *98* (2), 270–276. https://doi.org/10.1038/sj.bjc.6604158

Cheng, A.; Dixon, S. L. In silico models for the prediction of dose-dependent human hepatotoxicity. *J. Comput. Aided Mol. Des.* **2003**, *17* (12), 811–823. https://doi.org/10.1023/B:JCAM.0000021834.50768.c6

Collins, L. G.; Haines, C.; Perkel, R.; Enck, R. E. Lung cancer: Diagnosis and management. *Am. Fam. Physician.* **2007**, *75* (1), 56–63.

Daina, A.; Michielin, O.; Zoete, V. SwissADME: A free web tool to evaluate pharmacokinetics, drug-likeness and medicinal chemistry friendliness of small molecules. *Sci. Rep.* **2017**, *7*, 42717. https://doi.org/10.1038/srep42717

Darvas, F.; Keseru, G.; Papp, A.; Dorman, G.; Urge, L.; Krajcsi, P. In silico and ex silico ADME approaches for drug discovery. *Curr. Top. Med. Chem.* **2002**, *2* (12), 1287–1304. https://doi.org/10.2174/1568026023392841

Devesa, S. S.; Bray, F.; Vizcaino, A. P.; Parkin, D. M. International lung cancer trends by histologic type: Male:female differences diminishing and adenocarcinoma rates rising. *Int. J. Cancer.* **2005**, *117* (2), 294–299 https://doi.org/10.1002/ijc.21183

Dixon, S. L.; Smondyrev, A. M.; Knoll, E. H.; Rao, S. N.; Shaw, D. E.; Friesner, R. A. PHASE: A new engine for pharmacophore perception, 3D QSAR model development, and 3D database screening: 1. Methodology and preliminary results. *J. Comput. Aided Mol. Des.* **2006**, *20* (10–11), 647–671. https://doi.org/10.1007/s10822-006-9087-6

Faidallah, H. M.; Rostom, S. A. F. Synthesis, *in vitro* antitumor evaluation and DNA binding study of novel tetrahydroquinolines and some derived tricyclic and tetracyclic ring systems. *Eur. J. Med. Chem.* **2013**, *63*, 133–143. https://doi.org/10.1016/j.ejmech.2013.02.006

Fathy, U.; Azzam, M. A.; Mahdy, F.; El-Maghraby, S.; Allam, R. M. Synthesis and in vitro anticancer activity of some novel tetrahydroquinoline derivatives bearing pyrazol and hydrazide moiety. *J. Heterocycl. Chem.* **2020**, *57* (5), 2108–2120. https://doi.org/10.1002/jhet.3930

Grisoni, F.; Ballabio, D.; Todeschini, R.; Consonni, V. Molecular descriptors for structure–activity applications: A hands-on approach. In *Computational toxicology*. Nicolotti, O. Ed.; Humana Press, 2018; Vol. 1800, 3–53. https://doi.org/10.1007/978-1-4939-7899-1_1

Hayat, F.; Salahuddin, A.; Umar, S.; Azam, A. Synthesis, characterization, antiamoebic activity and cytotoxicity of novel series of pyrazoline derivatives bearing quinoline tail. *Eur. J. Med. Chem.* **2010**, *45* (10), 4669–4675. https://doi.org/10.1016/j.ejmech.2010.07.028

Hollenberg, P. F. Characteristics and common properties of inhibitors, inducers, and activators of CYP enzymes. *Drug Metab. Rev.* **2002**, *34* (1–2), 17–35. https://doi.org/10.1081/DMR-120001387

Ibrahim, M. T.; Uzairu, A.; Uba, S.; Shallangwa, G. A. Quantitative structure-activity relationship, molecular docking, drug-likeness, and pharmacokinetic studies of some non-small cell lung cancer therapeutic agents. *Beni-Suef Univ. J. Basic Appl. Sci.* **2020**, *9*, 49. https://doi.org/10.1186/s43088-020-00077-5

Johnson, T. O.; Adegboyega, A. E.; Iwaloye, O.; Eseola, O. A.; Plass, W.; Afolabi, B.; Rotimi, D.; Ahmed, E.; Albrakati, A.; Batiha, G. E.; Adeyemi, O. S. Computational study of the therapeutic potentials of a new series of imidazole derivatives against SARS-CoV-2. *J. Pharmacol. Sci.* **2021**, *147* (1), 62–71. https://doi.org/10.1016/j.jphs.2021.05.004

Lapa, G. B.; Bekker, O. B.; Mirchink, E. P.; Danilenko, V. N.; Preobrazhenskaya, M. N. Regioselective acylation of congeners of 3-amino-1H-pyrazolo[3,4-b]quinolines, their activity on bacterial serine/threonine protein kinases and in vitro antibacterial (including antimycobacterial) activity. *J. Enzyme Inhib. Med. Chem.* **2013**, *28* (5), 1088–1093. https://doi.org/10.3109/14756366.2012.716056

Lipinski, C. A.; Lombardo, F.; Dominy, B. W.; Feeney, P. J. Experimental and computational approaches to estimate solubility and permeability in drug discovery and development settings. *Adv. Drug Deliv. Rev.* **2001**, *46* (1–3), 3–26. https://doi.org/10.1016/S0169-409X(00)00129-0

Loving, K.; Salam, N. K.; Sherman, W. Energetic analysis of fragment docking and application to structure-based pharmacophore hypothesis generation. *J. Comput. Aided Mol. Des.* **2009**, *23* (8), 541–554. https://doi.org/10.1007/s10822-009-9268-1

Lynch, T.; Price, A. The effect of cytochrome P450 metabolism on drug response, interactions, and adverse effects. *Am. Fam. Physician*. **2007**, *76* (3), 391–396.

Mandewale, C. M.; Patil, U. C.; Shedge, S. V.; Dappadwad, U. R.; Yamgar, R. S. A review on quinoline hydrazone derivatives as a new class of potent antitubercular and anticancer agents. *Beni-Suef Univ. J. Basic Appl. Sci.* **2017**, *6* (4), 354–361. https://doi.org/10.1016/j.bjbas.2017.07.005

Mekheimer, R. A.; Al-Sheikh, M. A.; Medrasi, H. Y.; Sadek, K. U. Advancements in the synthesis of fused tetracyclic quinoline derivatives. *RSC Adv*. **2020**, *10* (34), 19867–19935. https://doi.org/10.1039/D0RA02786C

Morgensztern, D.; Ng, S. H.; Gao, F.; Govindan. R. Trends in stage distribution for patients with non-small cell lung cancer: A national cancer database survey. *J. Thorac. Oncol*. **2010**, *5* (1), 29–33. https://doi.org/10.1097/JTO.0b013e3181c5920c

Muegge, I.; Rarey, M. Small molecule docking and scoring. In *Computational chemistry review*. Lipkowitz, K. B., Boyd, D. B., Eds.; Wiley Online Library, 2001; Vol. 17, 1–60. https://doi.org/10.1002/0471224413.ch1

Ntie-Kang, F. An *in silico* evaluation of the ADMET profile of the StreptomeDB database. *SpringerPlus* **2013**, *2*, 353. https://doi.org/10.1186/2193-1801-2-353

Oke, A. M.; Adelakun, A. O.; Akintelu, S. A.; Soetan, E. A.; Oyebamiji, A. K.; Ewemoje, T. A. Inhibition of angiotensin converting enzyme by phytochemicals in *Cucurbita pepo* L.: *In silico Approach*. *Pharmacological Research - Modern Chinese Medicine.* **2022**, *4*, 100142. https://doi.org/10.1016/j.prmcm.2022.100142

Opoku-Temeng, C.; Dayal, N.; Sooreshjani, M. A.; Sintim, H. O. 3H-pyrazolo [4, 3-*f*] quinoline haspin kinase inhibitors and anticancer properties. *Bioorg. Chem.* **2018**, *78*, 418–426. https://doi.org/10.1016/j.bioorg.2018.03.031

Oyebamiji, A.K.; and Semire, B. Theoretical studies of anti-corrosion properties of triphenylimidazole derivatives in corrosion inhibition of carbon steel in acidic media via DFT approach. *Anal. Bioanal. Electrochem.* **2018**, *10* (1), 136–146.

Oyebamiji, A. K.; Fadare, O. A.; Akintelu, S. A; Semire, B. Biological studies on anthra[1,9-cd]pyrazol-6(2D)-one analogues as anti-vascular endothelial growth factor via in silico mechanisms. *Chemistry Africa* **2021**, *4* (4), 955–963. https://doi.org/10.1007/s42250-021-00276-2

Oyeneyin, O. E.; Iwegbulam, C. G.; Ipinloju, N.; Olajide, B. F.; Oyebamiji, A. K. Prediction of the antiproliferative effects of some benzimidazolechalcone derivatives against MCF-7 breast cancer cell lines: QSAR and molecular docking studies. *Org. Commun.* **2022**, *15* (3), 273–287. https://doi.org/10.25135/acg.oc.132.2203

Parr, R. G.; Szentpály, L.; Liu, S. Electrophilicity index. *J. Am. Chem. Soc.* **1999**, *121* (9), 1922–1924. https://doi.org/10.1021/ja983494x

Pettersen, E. F.; Goddard, T. D.; Huang, C. C.; Couch, G. S.; Greenblatt, D. M.; Meng, E. C.; Ferrin, T. E. UCSF Chimera—A visualization system for exploratory research and analysis. *J. Comput. Chem.* **2004**, *25* (13), 1605–1612. https://doi.org/10.1002/jcc.20084

Puzyn, T.; Leszczynski, J.; Cronin, M. *Recent Advances in QSAR Studies*: Methods and applications, Vol. 8; Springer Dordrecht, 2010. https://doi.org/10.1007/978-1-4020-9783-6

Sahin, S.; Benet, L. Z. The operational multiple dosing half-life: A key to defining drug accumulation in patients and to designing extended-release dosage forms. *Pharm. Res.* **2008**, *25* (12), 2869–2877. https://doi.org/10.1007/s11095-008-9787-9

Salim, E. I.; Jazieh, A. R.; Moore, M. A. Lung cancer incidence in the Arab League countries: Risk factors and control. *Asian Pacific J. Cancer Prev.* **2011**, *12* (1), 17–34.

Sato, T.; Watanabe, H.; Tsuganezawa, K.; Yuki, H.; Mikuni, J.; Yoshikawa, S.; Kukimoto-Niino, M.; Fujimoto, T.; Wakiyama, T. Y.; Kojim, H.; Okabe, T.; Nagano, T.; Shirouzu, M.; Yokoyama, S.; Tanaka, A.; Honma, T. Identification of novel drug-resistant EGFR mutant inhibitors by in silico screening using comprehensive assessments of protein structures. *Bioorg. Med. Chem.* **2012**, *20* (12), 3756–3767. https://doi.org/10.1016/j.bmc.2012.04.042

Semire, B.; Mutiu, O. A.; Oyebamiji, A. K. DFT and *AB INITIO* methods on NMR, IR and reactivity indices of indol-3-carboxylate and indazole-3-carboxylate derivatives of cannabinoids: Comparative study. *J. Phys. Theor. Chem.* **2017**, *13* (4), 353–377.

Siegel, R. L.; Miller, K. D.; Jemal, A. Cancer statistics, 2016. *CA: Cancer. J. Clin.* **2016,** *66* (1), 7–30. https://doi.org/10.3322/caac.21332

Stella, G. M.; Luisetti, M.; Inghilleri, S.; Cemmi, F.; Scabini, R.; Zorzetto, M.; Pozzi, E. Targeting EGFR in non-small-cell lung cancer: Lessons, experiences, strategies. *Respiratory Medicine* **2012,** *106* (2), 173–183. https://doi.org/10.1016/j.rmed.2011.10.015

Swierczewska, M.; Lee, K. C.; Lee, S. What is the future of PEGylated therapies? *Expert Opin. Emerg. Drugs* **2015**, *20* (4), 531–536. https://doi.org/10.1517/14728214.2015.1113254

Testa, B.; Krämer, S. D. The Biochemistry of Drug Metabolism – An Introduction: Part 5. Metabolism and Bioactivity. Chem. Biodivers. 2009, 6 (5), 591–684. https://doi.org/10.1002/cbdv.200900022

Trott, O.; Olson, A. J. AutoDock Vina: Improving the speed and accuracy of docking with a new scoring function, efficient optimization, and multithreading. *J. Comput. Chem.* **2010**, *31* (2), 455–461. https://doi.org/10.1002/jcc.21334

Vanommeslaeghe, K.; Guvench, O.; MacKerell Jr, A. D. Molecular mechanics. *Curr. Pharm. Des.* **2014**, *20* (20), 3281–3292. https://doi.org/10.2174/13816128113199990600

Veber, D. F.; Johnson, S. R.; Cheng, H.-Y.; Smith, B. R.; Ward, K. W.; Kopple, K. D. Molecular properties that influence the oral bioavailability of drug candidates. *J. Med. Chem.* **2002**, *45* (12), 2615–2623 https://doi.org/10.1021/jm020017n

Veerasamy, R.; Rajak, H.; Jain, A.; Sivadasan, S.; Varghese, C. P.; Agrawal, R. K. Validation of QSAR models - Strategies and importance. *Int. J. Drug Discov.* **2011**, *2* (3), 511–519.

Wang, H.; Liu, X.; Rice, S. J.; Belani, C. P. Pulmonary rehabilitation in lung cancer. *PM&R* **2016**, *8* (10), 990–996. https://doi.org/10.1016/j.pmrj.2016.03.010

Waziri, I.; Kelani, M. T.; Oyedeji-Amusa, M. O.; Oyebamiji, A. K.; Coetzee, L.-C. C.; Adeyinka, A. S.; Muller, A. J. Synthesis and computational investigation of *N,N* -dimethyl-4-[(Z)-(phenylimino)methyl]aniline derivatives: Biological and quantitative structural activity relationship studies. *J. Mol. Struct.* **2023**, *1276*, 134756. https://doi.org/10.1016/j.molstruc.2022.134756

Yang, L.; Feng, J.-K.; Ren, A.-M. Theoretical studies on the electronic and optical properties of two thiophene–fluorene based π-conjugated copolymers. *Polymer* **2005**, *46* (24), 10970–10981. https://doi.org/10.1016/j.polymer.2005.09.050

Yasuda, H.; Park, E.; Yun, C. H.; Sng, N. J.; Lucena-Araujo, A. R.; Yeo, W. L.; Huberman, M. S.; Cohen, D. W.; Nakayama, S.; Ishioka, K.; Yamaguchi, N.; Hanna, M.;

Oxnard, G. R.; Lathan, C. S.; Moran, T.; Sequist, L. V.; Chaft, J. E.; Riely, G. J.; Arcila, M. E.; Soo, R. A.; Meyerson, M.; Eck, M. J.; Kobayashi, S. S.; Costa, D. B. Structural, biochemical, and clinical characterization of epidermal growth factor receptor (EGFR) exon 20 insertion mutations in lung cancer. *Sci. Transl. Med.* **2013**, *5* (216), 216ra177. https://doi.org/10.1126/scitranslmed.3007205

Zhang, Z.; Lee, J. C.; Lin, L.; Olivas, V.; Au, V.; LaFramboise, T.; Abdel-Rahman, M.; Wang, X.; Levine, A. D.; Rho, J. K.; Choi, Y. J.; Choi, C. M.; Kim, S. W.; Jang, S. J.; Park, Y. S.; Kim, W. S.; Lee, D. H.; Lee, J. S.; Miller, V. A.; Arcila, M.; Ladanyi, M.; Moonsamy, P.; Sawyers, C.; Boggon, T. J.; Ma, P. C.; Costa, C.; Taron, M.; Rosell, R.; Halmos, B.; Bivona, T. G. Activation of the AXL kinase causes resistance to EGFR-targeted therapy in lung cancer. *Nat. Genet.* **2012**, *44* (8), 852–860. https://doi.org/10.1038/ng.2330